ChemComm

COMMUNICATION

View Article Online
View Journal | View Issue

Cite this: *Chem. Commun.*, 2023, 59, 4966

Received 23rd February 2023,
Accepted 29th March 2023

DOI: 10.1039/d3cc00855j

rsc.li/chemcomm

CAl_{11}^-: a molecular rotor with a quasi-planar tetracoordinate carbon†

Li-Xia Bai,[a] Jorge Barroso,[b] Mesías Orozco-Ic,[c] Filiberto Ortiz-Chi,[d] Jin-Chang Guo *[a] and Gabriel Merino *[b]

In this work, we analyzed the bonding and fluxional character of the global minimum of CAl_{11}^-. Its structure is formed by two stacked layers, one of them resembles the well-known planar tetracoordinate carbon CAl_4 on top of a hexagonal $Al@Al_6$ wheel. Our results show that the CAl_4 fragment rotates freely around the central axis. The exceptional stability and fluxionality of CAl_{11}^- derive from its particular electron distribution.

In principle, boron and aluminum are similar. Both belong to the same group in the periodic table with comparable electronegativity values. The major distinction is their size; the covalent radius of boron is about 30% smaller, which along with its electron deficiency, plays a crucial role in its structural diversity. In fact, the architectural zoo is so vast that boron clusters stand out for their unusual chemical bonding, aromaticity, and fluxionality.[1–4] In 2010, the first case of fluxionality in boron clusters was published, B_{19}^-.[5,6] In this system, an inner B_6 fragment rotates freely within the peripheral B_{13} ring, mimicking a rotary internal-combustion engine, hence the name of the molecular Wankel rotor. Shortly after, similar dynamic behavior in other boron clusters was discovered.[7–12] The most renowned case is B_{13}^+ because its fluxionality was experimentally corroborated by cryogenic ion vibrational spectroscopy,[13] and it has been used to study how to control the internal rotation by circularly polarized laser radiation.[14]

The fluxionality is not exclusive to bare boron clusters.[15–17] We recently introduced $B_3Al_4^+$.[18] This system is formed by a triangular B_3 unit rotating on top of an Al_4 square, simulating the motion of a three-dimensional Reuleaux triangle. This has motivated us to reconsider designing molecular rotors based on aluminum clusters. This is a complex task. In essence, fluxionality in boron clusters is primarily driven by the multicenter nature of their chemical bonds, *i.e.*, doping or replacing boron with other atoms might shut down such dynamic behavior. For example, substituting a single boron with a carbon atom in B_{19}^- and B_{11}^- stops the rotation due to the formation of a localized σ-bond.[19,20] This may suggest that clusters with carbon elude this type of fluxional behavior.

Recently, Zheng *et al.* studied a series of clusters CAl_n^- (n = 6–15).[21] According to their photoelectron spectroscopy study, in conjunction with a global minimum computational search, CAl_{11}^- is formed by a CAl_4 unit on top of a hexagonal $Al@Al_6$ quasi-planar fragment. In other words, it is another two-layer system resembling the $B_3Al_4^+$ Reuleaux triangle.[22–25] Noticeably, one of the layers in CAl_{11}^- resembles the well-known CAl_4^{2-}, which is one of the most studied planar tetracoordinate carbons (ptCs) with aluminum.[26–28] Can CAl_{11}^-, a system with a ptC already experimentally detected in the gas phase, be fluxional? In this study, we analyze the bonding nature and fluxional character of CAl_{11}^-. Our results show that the CAl_4 unit rotates freely around the central axis, implying that CAl_{11}^- is the first aluminum-based ptC molecular rotor.

To identify the energetic landscape of CAl_{11}^-, the exploration of its potential energy surface (PES) for singlet and triplet states was carried out through coalescence kick and genetic algorithms.[29,30] An initial screening was done at the PBE0/3-21G level.[31] The twenty lowest-lying energy isomers were re-minimized at the PBE0/def2-QZVP level.[32] The vibrational frequencies were computed at the same level to characterize the nature of the stationary points. Relative energies for the four lowest-energy isomers were refined using single-point CCSD(T)/def2-QZVP computations,[33] including the ZPE corrections at the PBE0/def2-QZVP level. Thus, the energy discussion is based on the CCSD(T)/def2-QZVP//PBE0/def2-QZVP results. All these computations were conducted with Gaussian 16.[34] Wiberg Bond Index (WBI) and Natural Population Analysis

[a] *Nanocluster Laboratory, Institute of Molecular Science, Shanxi University, Taiyuan 030006, China. E-mail: guojc@sxu.edu.cn*
[b] *Departamento de Física Aplicada, Centro de Investigación y de Estudios Avanzados, Unidad Mérida. Km 6 Antigua Carretera a Progreso. Apdo. Postal 73, Cordemex, 97310, Mérida, Yuc, Mexico. E-mail: gmerino@cinvestav.mx*
[c] *Department of Chemistry, Faculty of Science, University of Helsinki, P.O. Box 55, A. I. Virtasen aukio 1, FIN-00014, Helsinki, Finland*
[d] *CONACYT-División Académica de Ciencias Básicas, Universidad Juárez Autónoma de Tabasco, Cunduacán 86690, Tabasco, Mexico*

† Electronic supplementary information (ESI) available: Supplementary Table S1, Fig. S1–S3, and one BOMD movie. See DOI: https://doi.org/10.1039/d3cc00855j

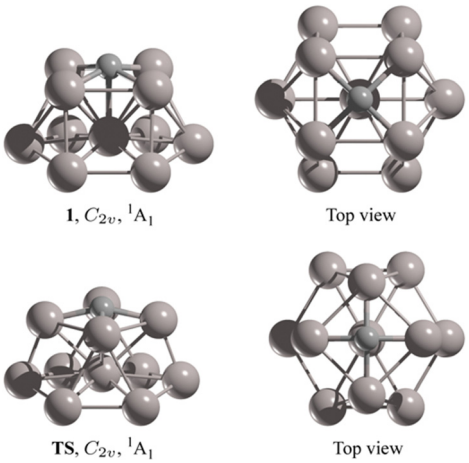

Fig. 1 Side and top views of the global minimum and transition state of the CAl_{11}^- global minimum.

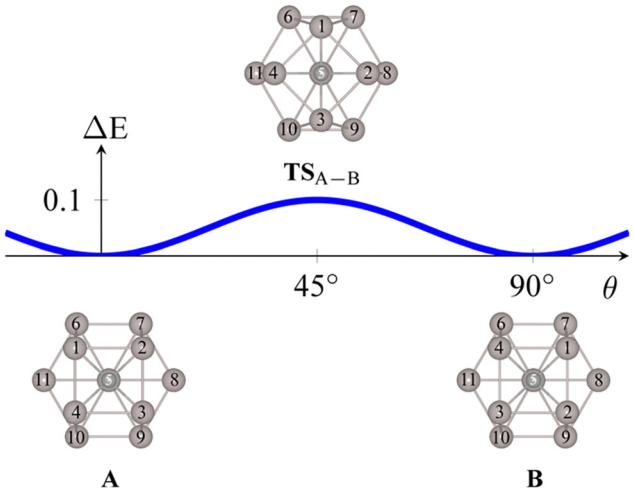

Fig. 2 Rotational mechanism of CAl_{11}^-.

(NPA) were estimated following the NBO6 scheme.[35] The adaptive natural density partitioning (AdNDP)[36] analysis was done using the Multiwfn program.[37] For a better understanding of electron delocalization, the magnetically induced current density ($\mathbf{J}^{ind}$) and the induced magnetic field ($\mathbf{B}^{ind}$) were estimated using the GIMIC[38] and Aromagnetic[39] programs, respectively. The orbital contribution to $\mathbf{B}^{ind}$ was determined through NCS analysis.[40] To assess the contribution of core electrons to the magnetic response, the removing valence electron method was utilized.[41] The dynamical behavior of CAl_{11}^- was confirmed by Born-Oppenheimer Molecular Dynamics (BOMD)[42] simulations at temperatures of 300 and 500 K at the PBE0/6-31G(d) level. Each simulation ran for 30 ps with a step size of 2.2 fs from the equilibrium global minimum structure with random velocities assigned to the atoms according to a Maxwell–Boltzmann distribution for both temperatures and then normalized so that the net moment for the whole system is zero.

Fig. 1 shows the top and side views of the global minimum of CAl_{11}^-, **1**. The relative energy between **1** and the nearest local minimum is 5.8 kcal mol^{-1}. Fig. S1 (ESI†) includes the remaining low-lying isomers. The structure of **1** adopts C_{2v} symmetry with two stacked layers (with a C-Al interlayer spacing of 2.31 Å), a planar CAl_4 quasi-square (carbon is just 0.41 Å above the Al_4 plane) on top of a hexagonal $Al@Al_6$ wheel. The C-Al bond lengths in the CAl_4 framework are 1.99 Å, just 0.03 Å longer than in D_{4h} CAl_4^{2-} and halfway between the lengths in C_{2v} CAl_4^- (1.95 and 2.00 Å, respectively). The Al–Al distances, including those between layers, range between 2.66 and 2.83 Å, similar to those in CAl_4^{2-} (2.87 Å) and CAl_4^- (2.69–2.93 Å).

According to NBO analysis (Fig. S2, ESI†), the negative charge (-0.5 $|e|$) is spread evenly across the two fragments. Remarkably, the ptC has a natural charge of -2.4 $|e|$, which is identical to other ptC clusters such as CAl_4^{2-}. With respect to the Wiberg bond indices, the corresponding values in the CAl_4 unit are 0.44 for C–Al and 0.26–0.32 for Al–Al (Fig. S2, ESI†). In contrast, the WBI_{Al-Al} at the Al_7 periphery range from 0.64 to 0.72, and 0.40 for the radial Al–Al bonds. This indicates a stronger electron localization in the perimeter of the Al_7 ring, *i.e.*, a higher covalent character in the outer Al–Al bonds. Moreover, the values between layers are significant. Specifically, the WBI_{C-Al} between layers is 0.42, while the WBI_{Al-Al} is 0.40–0.62, implying a considerable interaction between the two moieties.

So far, we have described the structure of CAl_{11}^- including some details to understand how the fragments are bound; nothing different from what Zheng *et al.* reported. The oddity emerges by inspecting the frequency analysis. There is a soft mode of just 23 cm^{-1} associated with the rotation of the CAl_4 moiety around the central axis of the Al_7 wheel (Fig. S3, ESI†). This implies that the system may be fluxional. In fact, there is a transition state (**TS**) with an imaginary frequency (ν_{min} = 18*i* cm^{-1}) corresponding to a 45° rotation of the CAl_4 fragment (Fig. 2). Such **TS** also has C_{2v} symmetry and is just 0.1 kcal mol^{-1} above **1**! The structural parameters, WBIs, and atomic charges of **TS** are quite similar to those of **1** (Fig. S2, ESI†).

BOMD simulations were performed at the PBE0/6-31G(d) level to corroborate the dynamic fluxionality of the global minimum of CAl_{11}^-. The simulations, at 300 and 500 K, confirm the rotation around the central axis of the CAl_4 framework. The rotation resembles a molecular rotor from the top view. A short movie with a simulation of over 30 ps at 500 K is included as an example in the ESI.† Both layers in CAl_{11}^- maintained their structural integrity, *i.e.*, no fragment dissociation or significant distortion was perceptible.

The charge distribution and bond orders indicate that the two pieces interact significantly. So, why does CAl_{11}^- exhibit such unusual dynamic behavior? AdNDP (Fig. 3) reveals three delocalized 5c–2e σ-bonds within the CAl_4 fragment, and a delocalized 6c–2e π-bond involving the carbon and the central Al atom of the Al_7 wheel. In addition, there are six localized 2c–2e Al–Al σ-bonds at the perimeter of the Al_7 ring and three radial σ-bonds entirely delocalized. Besides the delocalized 6c–2e π-bond, the interaction between layers is recovered by the AdNDP through four 2c–2e Al–Al and two 3c–2e σ-bonds. This is relevant for fluxionality since only the interlayer bonds change during the rotation process. Specifically, four 2c–2e Al–Al σ-bonds in **1** evolved into four delocalized 3c–2e σ-bonds in **TS**, while the two interlayer 3c–2e σ-bonds in **1** become 2c–2e bonds in **TS**. This process happens every 45° (Fig. 2).

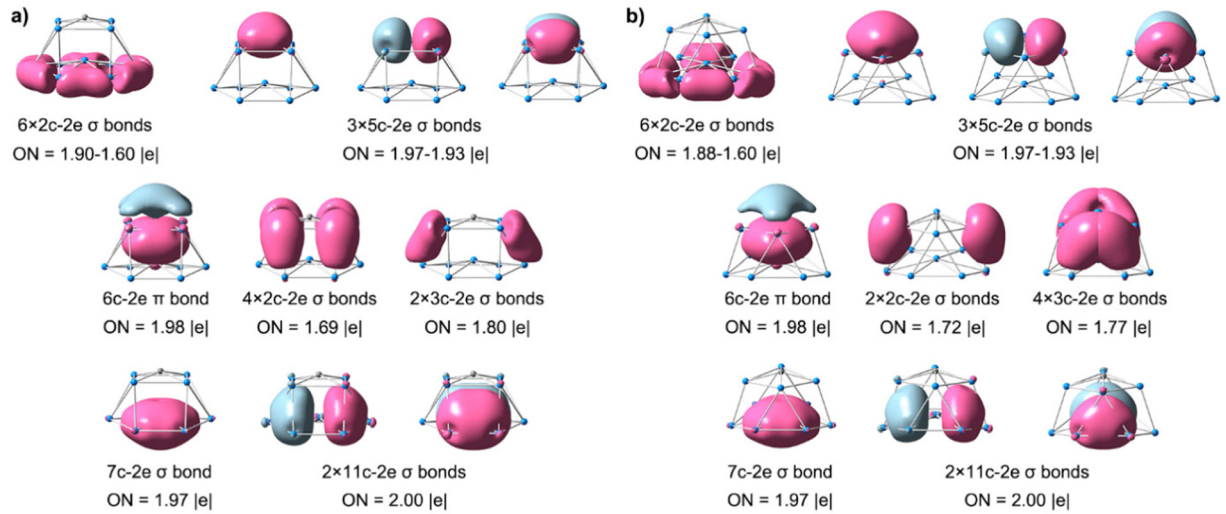

Fig. 3 The adaptive natural density partitioning (AdNDP) analysis for **1** (left) and **TS** (right). The occupation numbers (ONs) are shown.

In summary, the main components remain unchanged as the connectivity between them changes from localized to delocalized and *vice versa*.

Electron delocalization of CAl_{11}^- is examined by its magnetic response to an external magnetic field parallel to the rotation axis (Fig. 4). An entirely diatropic ring current flows clockwise in and between layers. Concomitantly, this current creates a $\mathbf{B}^{ind}$, whose main component, the *z*-component (B_z^{ind}), reveals that the cluster is strongly shielded due to the σ-electrons (B_z^{ind} values even lower than −50 ppm). The π-electrons also contribute to the shielding, but weakly. Analysis of the ring current shows that the strongest $\mathbf{J}^{ind}$ flux is near the Al_7 wheel. The $\mathbf{J}^{ind}$ integration results in a global ring current strength of 91.3 nA T^{-1}. However, the magnetic response is contaminated by the core electrons, especially near the nuclei. Because the integration plane crosses two nuclei, it is best to disregard their contribution. As a result, subtracting the intensity of the core electrons (28.19 nA T^{-1}) from the total yields 63 nA T^{-1}. This suggests that the system is highly delocalized, with a ring current five times stronger than that of benzene (12 nA T^{-1}).

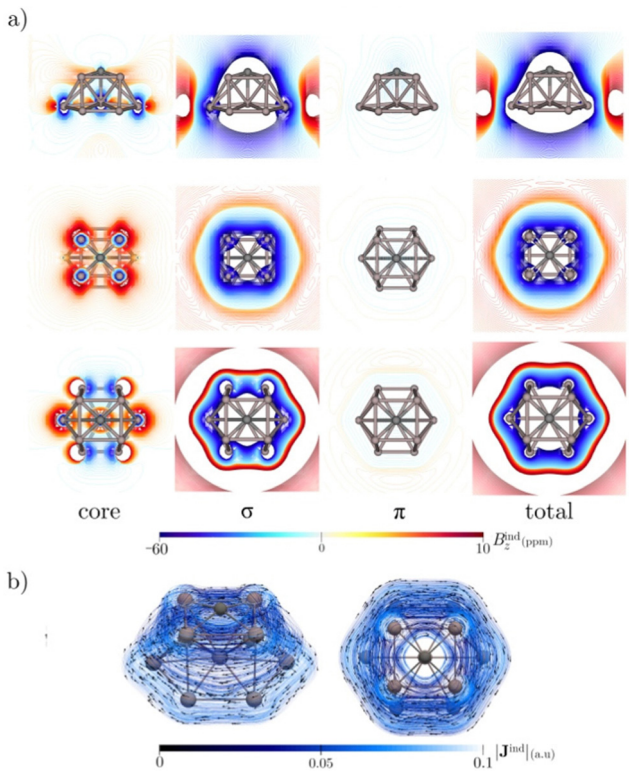

Fig. 4 (a) B_z^{ind} isolines plotted in the plane of the Al_7 (bottom), of the CAl_4 framework (middle), and in a transverse plane (top) to CAl_{11}^-. (b) $\mathbf{J}^{ind}$ maps plotted near CAl_{11}^-. The arrows indicate the direction of the current density. The $|\mathbf{J}^{ind}|$ scale is in atomic units (1 a.u. = 100.63 nA T^{-1} $Å^{-2}$).

In summary, the structure of CAl_{11}^- consists of two stacked layers; one is a CAl_4 framework containing a quasi-planar tetracoordinate carbon on a hexagonal Al_7 wheel. Our computations revealed that, although there is strong contact between the two layers, there are almost no barriers to the rotation of one over the other. BOMD simulations show that the dynamic behavior occurs without severe distortions. Along the rotation, both fragments remain unchanged as the connectivity between them changes from localized to delocalized and *vice versa*. So, CAl_{11}^- is the first aluminum-based ptC molecular rotor with outstanding stability and fluxionality.

This work is supported by the National Natural Science Foundation of China (22173053), the Natural Science Foundation of Shanxi Province (20210302123439). M.O.-I. thanks the Magnus Ehrnrooth Foundation for the financial support.

Conflicts of interest

There are no conflicts to declare.

Notes and references

1 T. Jian, X. Chen, S. D. Li, A. I. Boldyrev, J. Li and L. S. Wang, *Chem. Soc. Rev.*, 2019, **48**, 3550–3591.
2 J. Barroso, S. Pan and G. Merino, *Chem. Soc. Rev.*, 2022, **51**, 1098–1123.

3 S. Jalife, L. Liu, S. Pan, J. L. Cabellos, E. Osorio, C. Lu, T. Heine, K. J. Donald and G. Merino, *Nanoscale*, 2016, **8**, 17639–17644.
4 S. Pan, J. Barroso, S. Jalife, T. Heine, K. R. Asmis and G. Merino, *Acc. Chem. Res.*, 2019, **52**, 2732–2744.
5 W. Huang, A. P. Sergeeva, H. J. Zhai, B. B. Averkiev, L. S. Wang and A. I. Boldyrev, *Nat. Chem.*, 2010, **2**, 202–206.
6 J. O. C. Jiménez-Halla, R. Islas, T. Heine and G. Merino, *Angew. Chem., Int. Ed.*, 2010, **49**, 5668–5671.
7 G. Martínez-Guajardo, A. P. Sergeeva, A. I. Boldyrev, T. Heine, J. M. Ugalde and G. Merino, *Chem. Commun.*, 2011, **47**, 6242–6244.
8 G. Merino and T. Heine, *Angew. Chem., Int. Ed.*, 2012, **51**, 10226–10227.
9 D. Moreno, S. Pan, L. L. Zeonjuk, R. Islas, E. Osorio, G. Martínez-Guajardo, P. K. Chattaraj, T. Heine and G. Merino, *Chem. Commun.*, 2014, **50**, 8140–8143.
10 T. B. Tai, A. Ceulemans and M. T. Nguyen, *Chem. – Eur. J.*, 2012, **18**, 4510–4512.
11 Y. J. Wang, X. Y. Zhao, Q. Chen, H. J. Zhai and S. D. Li, *Nanoscale*, 2015, **7**, 16054–16060.
12 Y. J. Wang, X. R. You, Q. Chen, L. Y. Feng, K. Wang, T. Ou, X. Y. Zhao, H. J. Zhai and S. D. Li, *Phys. Chem. Chem. Phys.*, 2016, **18**, 15774–15782.
13 M. R. Fagiani, X. Song, P. Petkov, S. Debnath, S. Gewinner, W. Schöllkopf, T. Heine, A. Fielicke and K. R. Asmis, *Angew. Chem., Int. Ed.*, 2017, **56**, 501–504.
14 J. Zhang, A. P. Sergeeva, M. Sparta and A. N. Alexandrova, *Angew. Chem., Int. Ed.*, 2012, **51**, 8512–8515.
15 J. C. Guo, L. Y. Feng, Y. J. Wang, S. Jalife, A. Vásquez-Espinal, J. L. Cabellos, S. Pan, G. Merino and H. J. Zhai, *Angew. Chem., Int. Ed.*, 2017, **56**, 10174–10177.
16 W. L. Li, T. Jian, X. Chen, H. R. Li, T. T. Chen, X. M. Luo, S. D. Li, J. Li and L. S. Wang, *Chem. Commun.*, 2017, **53**, 1587–1590.
17 R. Yu, J. Barroso, M. Wang, W. Liang, C. Chen, X. Zarate, M. Orozco-Ic, Z. Cui and G. Merino, *Phys. Chem. Chem. Phys.*, 2020, **22**, 12312–12320.
18 L. X. Bai, M. Orozco-Ic, X. Zarate, D. Sundholm, S. Pan, J. C. Guo and G. Merino, *Molecules*, 2022, **27**, 7407.
19 F. Cervantes-Navarro, G. Martínez-Guajardo, E. Osorio, D. Moreno, W. Tiznado, R. Islas, K. J. Donald and G. Merino, *Chem. Commun.*, 2014, **50**, 10680–10682.
20 Y. J. Wang, J. C. Guo and H. J. Zhai, *Nanoscale*, 2017, **9**, 9310–9316.
21 C. J. Zhang, W. S. Dai, H. G. Xu, X. L. Xu and W. J. Zheng, *J. Phys. Chem. A*, 2022, **126**, 5621–5631.
22 R. Hoffmann, R. W. Alder and C. F. Wilcox, *J. Am. Chem. Soc.*, 1970, **92**, 4992–4993.
23 R. Keese, *Chem. Rev.*, 2006, **106**, 4787–4808.
24 L. Yang, E. Ganz, Z. Chen, Z. Wang and P. V. R. Schleyer, *Angew. Chem., Int. Ed.*, 2015, **54**, 9468–9501.
25 G. Merino, M. A. Méndez-Rojas, A. Vela and T. Heine, *J. Comput. Chem.*, 2007, **28**, 362–372.
26 X. Li, L. S. Wang, A. I. Boldyrev and J. Simons, *J. Am. Chem. Soc.*, 1999, **121**, 6033–6038.
27 X. Li, H. F. Zhang, L. S. Wang, G. D. Geske and A. I. Boldyrev, *Angew. Chem., Int. Ed.*, 2000, **39**, 3630–3632.
28 A. C. Castro, M. Audiffred, J. M. Ugalde, M. A. Méndez-Rojas and G. Merino, *Chem. Phys. Lett.*, 2012, **519**, 29–33.
29 A. P. Sergeeva, B. B. Averkiev, H. J. Zhai, A. I. Boldyrev and L. S. Wang, *J. Chem. Phys.*, 2011, **134**, 224304.
30 F. Ortiz-Chi and G. Merino, *GLOMOS*, Mérida, México, 2020.
31 C. Adamo and V. Barone, *J. Chem. Phys.*, 1999, **110**, 6158–6170.
32 F. Weigend and R. Ahlrichs, *Phys. Chem. Chem. Phys.*, 2005, **7**, 3297–3305.
33 G. D. Purvis III and R. J. Bartlett, *J. Chem. Phys.*, 1982, **76**, 1910–1918.
34 M. J. Frisch, G. W. Trucks, H. B. Schlegel, G. E. Scuseria, M. A. Robb, J. R. Cheeseman, G. Scalmani, V. Barone, B. Mennucci, G. A. Petersson, H. Nakatsuji, M. Caricato, X. Li, H. P. Hratchian, A. F. Izmaylov, J. Bloino, G. Zheng, J. L. Sonnenberg, M. Hada, M. Ehara, K. Toyota, R. Fukuda, H. Borkent, W. Laarhoven, J. Hasegawa, M. Ishida, T. Nakajima, Y. Honda, O. Kitao, H. Nakai, T. Vreven, J. J. Montgomery, J. E. Peralta, F. Ogliaro, M. Bearpark, J. J. Heyd, E. Brothers, K. N. Kudin, V. N. Staroverov, R. Kobayashi, J. Normand, K. Raghavachari, A. Rendell, J. C. Burant, S. S. Iyengar, J. Tomasi, M. Cossi, N. Rega, N. J. Millam, M. Klene, J. E. Knox, J. B. Cross, V. Bakken, C. Adamo, J. Jaramillo, R. Gomperts, R. E. Stratmann, O. Yazyev, A. J. Austin, R. Cammi, C. Pomelli, J. W. Ochterski, R. L. Martin, K. Morokuma, V. G. Zakrzewski, G. A. Voth, P. Salvador, J. J. Dannenberg, S. Dapprich, D. Daniels, O. Farkas, J. B. Foresman, J. V. Ortiz, J. Cioslowski and D. J. Fox, *Gaussian 16, Revision C.01*, Gaussian, Inc., Wallingford, CT, 2016.
35 E. D. Glendening, C. R. Landis and F. Weinhold, *J. Comput. Chem.*, 2013, **34**, 1429–1437.
36 D. Y. Zubarev and A. I. Boldyrev, *Phys. Chem. Chem. Phys.*, 2008, **10**, 5207–5217.
37 T. Lu and F. Chen, *J. Comput. Chem.*, 2012, **33**, 580–592.
38 J. Jusélius, D. Sundholm and J. Gauss, *J. Chem. Phys.*, 2004, **121**, 3952–3963.
39 M. Orozco-Ic, J. L. Cabellos and G. Merino, *Aromagnetic*, Cinvestav-Mérida, Mexico, 2016.
40 J. A. Bohmann, F. Weinhold and T. C. Farrar, *J. Chem. Phys.*, 1997, **107**, 1173–1184.
41 M. Orozco-Ic, N. D. Charistos, A. Munoz-Castro, R. Islas, D. Sundholm and G. Merino, *Phys. Chem. Chem. Phys.*, 2022, **24**, 12158–12166.
42 J. M. Millam, V. Bakken, W. Chen, W. L. Hase and H. B. Schlegel, *J. Chem. Phys.*, 1999, **111**, 3800–3805.